Automatica 107 (2019) 483–492

Contents lists available at ScienceDirect

Automatica

journal homepage: www.elsevier.com/locate/automatica

Brief paper

Reset integral control for improved settling of PID-based motion systems with friction☆

R. Beerens [a,*], A. Bisoffi [b], L. Zaccarian [c,d], W.P.M.H. Heemels [a], H. Nijmeijer [a], N. van de Wouw [a,e]

[a] Eindhoven University of Technology, Department of Mechanical Engineering, 5600MB Eindhoven, The Netherlands
[b] KTH Royal Institute of Technology, Division of Decision and Control Systems, SE-10044 Stockholm, Sweden
[c] CNRS, LAAS, Univ. de Toulouse, 31400 Toulouse, France
[d] University of Trento, 38122 Trento, Italy
[e] University of Minnesota, Civil, Environmental & Geo-Engineering Department, MN 55455, USA

ARTICLE INFO

Article history:
Received 15 March 2018
Received in revised form 6 May 2019
Accepted 7 June 2019
Available online xxxx

Keywords:
Transient performance
Hybrid control
Motion control
Friction
Stability

ABSTRACT

We present a reset control approach to improve the transient performance of a PID-controlled motion system subject to Coulomb and viscous friction. A reset integrator is applied to circumvent the depletion and refilling process of a linear integrator when the solution overshoots the setpoint, thereby significantly reducing the settling time. Robustness for unknown static friction levels is obtained. The closed-loop system is formulated through a hybrid systems framework, within which stability is proven using a discontinuous Lyapunov-like function and a meagre-limsup invariance argument. The working principle of the proposed reset controller is analyzed in an experimental benchmark study of an industrial high-precision positioning machine.

1. Introduction

In this paper, we present a reset integral control approach to improve settling (transient) performance of a PID-controlled mechanical motion system subject to friction. Friction is a performance-limiting factor in many high-precision positioning systems, in the sense of, e.g., achievable setpoint accuracy and settling times. Control of motion systems with friction has been an active field of research in the past decades, and many different control solutions have been developed. Several control approaches rely on developing as-accurate-as-possible friction models in order to compensate for friction in the control loop, see, e.g., Armstrong-Hélouvry, Dupont, and Canudas de Wit (1994), Freidovich, Robertsson, Shiriaev, and Johansson (2010) and Makkar, Hu, Sawyer, and Dixon (2007) and the references therein. However, model-based friction compensation techniques may suffer from over- and undercompensation of friction due to unreliable friction measurements, uncertainties in the friction characteristic, and model mismatches. Consequently, the system may exhibit limit cycles or nonzero steady-state errors (thereby losing stability of the setpoint), as thoroughly analyzed in Putra, Nijmeijer, and van de Wouw (2007). Non-model-based control techniques do not aim at friction compensation using a friction model, but change the response by applying specific control signals, thereby obtaining the desired performance despite the apparent friction. Examples of such techniques are impulsive control (see, e.g., Orlov, Santiesteban, & Aguilar, 2009; van de Wouw & Leine, 2012), dithering-based techniques (see, e.g., Iannelli, Johansson, Jönsson, & Vasca, 2006; Thomsen, 1999), or (second-order) sliding mode control (see, e.g., Bartolini, Pisano, Punta, & Usai, 2003). In general, these non-model-based control techniques have a common disadvantage. Namely, the persistent injection of high-frequency control signals may excite unmodeled high-frequency system dynamics, which is highly undesirable in motion systems, and, therefore, these techniques are not appealing for being used in industrial applications.

Despite the existence of the above control techniques, linear controllers are still applied in the vast majority of industrial motion systems. Control practitioners are often well-trained in linear control design (loop-shaping), and the existence of

☆ This work is part of the research programme CHAMeleon with project number 13896, which is (partly) financed by the Netherlands Organisation for Scientific Research (NWO). Research was supported in part by ANR via grant HANDY, number ANR-18-CE40-0010. The material in this paper was partially presented at the 2018 American Control Conference, June 27–29, 2018, Milwaukee, USA. This paper was recommended for publication in revised form by Associate Editor Warren E. Dixon under the direction of Editor Daniel Liberzon.

* Corresponding author.
E-mail addresses: r.beerens@tue.nl (R. Beerens), bisoffi@kth.se (A. Bisoffi), zaccarian@laas.fr (L. Zaccarian), w.p.m.h.heemels@tue.nl (W.P.M.H. Heemels), h.nijmeijer@tue.nl (H. Nijmeijer), n.v.d.wouw@tue.nl (N. van de Wouw).

https://doi.org/10.1016/j.automatica.2019.06.017

intuitive tuning tools for linear controllers makes them undiminishedly popular. In particular, the classical proportional–integral–derivative (PID) controller is most commonly used for frictional systems, since the integrator action results in compensation of unknown static friction by integrating the position error. However, PID control is prone to performance limitations as well. Firstly, the integrator action in the presence of the velocity-weakening (i.e., Stribeck) effect may induce limit cycling (*hunting*), thereby losing asymptotic stability of the setpoint (Armstrong-Hélouvry et al., 1994; Hensen, van de Molengraft, & Steinbuch, 2003). A second limitation is the slow convergence (and resulting long settling times) in the presence of static friction, see, e.g., Bisoffi, Da Lio, Teel, and Zaccarian (2018, Remark 3). Integrator action is required to escape a stick phase by building up the control force to overcome the (possibly unknown) static friction. However, if the system overshoots the setpoint, the control signal must be pointed in the reverse direction to overcome the static friction again. To this end, the integrator buffer needs to deplete and refill. Despite achieving stability of the setpoint, this process takes increasingly more time with a decreasing position error. This results in long settling times, adversely affecting the machine throughput.

In this paper, we address the second limitation in the context of PID control. In particular, we propose a reset integral control scheme that significantly improves transient performance in terms of settling time, and is applicable as an add-on to loop-shaped PID controllers, as designed for industrial motion applications. By building upon a well-known control strategy embraced by the industry, we aim at reducing the threshold for control engineers to use a nonlinear control technique in an industrial environment. Inspired by the Clegg integrator (Clegg, 1958) and the First Order Reset Element (Horowitz & Rosenbaum, 1975), reset controllers have been used to increase performance in (linear) motion control applications (see, e.g., Aangenent, Witvoet, Heemels, van de Molengraft, & Steinbuch, 2010; Deenen, Heertjes, Heemels, & Nijmeijer, 2017; El Rifai & El Rifai, 2009; van Loon, Hunnekens, Heemels, van de Wouw, & Nijmeijer, 2016; Nešić, Teel, & Zaccarian, 2011 and van Loon, Gruntjens, Heertjes, van de Wouw, & Heemels, 2017; Nešić, Zaccarian, & Teel, 2008 for corresponding analysis tools), or disturbance attenuation (see Zhao & Wang, 2016). To the best of the authors' knowledge, however, reset integrators have not yet been applied to improve settling performance of nonlinear systems with friction.

The main contributions of this paper are as follows. The first one is a novel reset control design for systems with friction that both improves transient performance with respect to a classical PID controller, and achieves robust stability with respect to uncertainties in the static friction. The reset mechanism is robust to velocity measurement noise, and can be readily made robust for asymmetric static friction, if needed. Moreover, the proposed controller minimizes the risk of exciting unmodeled high-frequency dynamics, despite the presence of a discontinuous control signal, thereby addressing a major concern of control engineers in industry. The second contribution is the stability analysis of the resulting *hybrid* closed-loop system, which exploits a meagre-limsup invariance argument (Goebel, Sanfelice, & Teel, 2012, §8.4). The third contribution is a demonstration of the transient performance improvements using the proposed reset control architecture by means of a case study on an industrial high-precision positioning application (a manipulation stage of an electron microscope). This paper builds upon our previous work in Beerens et al. (2018), which contains the controller design and a simulation example. In addition to Beerens et al. (2018), this paper contains a more general controller reset law, proofs, and experimental results.

The paper is organized as follows. In Section 2, a model of the considered motion system with a classical PID controller is presented together with the reset integrator control law. The closed-loop dynamics are written in a hybrid systems formalism in Section 3 and a stability analysis is given in Section 4. In Section 5, a case study on a high-precision positioning application is discussed, and conclusions are presented in Section 6.

Notation: $\operatorname{sign}(\cdot)$ (with a lower-case s) denotes the classical sign function, i.e., $\operatorname{sign}(y) := y/|y|$ for $y \neq 0$ and $\operatorname{sign}(0) := 0$. $\operatorname{Sign}(\cdot)$ (with an upper-case S) denotes the *set-valued* sign function, i.e., $\operatorname{Sign}(y) := \{\operatorname{sign}(y)\}$ for $y \neq 0$, and $\operatorname{Sign}(y) := [-1, 1]$ for $y = 0$. For $c > 0$, the deadzone function is defined as: $\mathrm{dz}_c(x) := 0$ if $|x| \leq c$, $\mathrm{dz}_c(x) := x - c$ if $x > c$, $\mathrm{dz}_c(x) := x + c$ if $x < -c$. A function $f : D \to \mathbb{R}$ is lower semicontinuous if $\liminf_{x \to x_0} f(x) \geq f(x_0)$ for each point x_0 in its domain D. The lower right Dini derivative D_+h of a function h is defined as $D_+h(t) := \liminf_{\epsilon \to 0^+} \frac{h(t+\epsilon)-h(t)}{\epsilon}$. The logical OR and AND are denoted by $\vee$ and $\wedge$, respectively.

2. Reset integral control design

In this section, we describe the motion system with friction, and discuss the design of the reset control law.

Consider a single-degree-of-freedom mass m sliding on a horizontal plane with position z_1 and velocity z_2. The mass is subject to a control input $\bar{u}$ and a friction force belonging to a friction set $\Psi(z_2)$ for a velocity z_2, where $z_2 \rightrightarrows \Psi(z_2)$ is a set-valued mapping. The system dynamics are then given by the differential inclusion

$$\dot{z}_1 = z_2, \quad \dot{z}_2 \in \tfrac{1}{m}\left(\Psi(z_2) + \bar{u}\right). \tag{1}$$

The set-valued friction characteristic Ψ consists of Coulomb friction with *unknown* static friction $\bar{F}_s$, and a viscous contribution γz_2, where $\gamma \geq 0$ is the viscous friction coefficient:

$$\Psi(z_2) := -\bar{F}_s \operatorname{Sign}(z_2) - \gamma z_2. \tag{2}$$

Since the current paper is primarily focused on robust compensation of unknown Coulomb friction and on transient performance improvement, we have assumed that a velocity-weakening (Stribeck) effect is absent in the friction characteristic Ψ (in the presence of such an effect, a velocity-dependent compensation control term may be employed as in Beerens, Nijmeijer, Heemels, and van de Wouw (2017)). The goal is to control the mass to the constant setpoint $(z_1, z_2) = (r, 0)$.

Let us formulate the control problem of this paper.

Problem 1. Design a *reset* PID controller for input $\bar{u}$ in (1)–(2) that (1) globally asymptotically stabilizes the setpoint $(z_1, z_2) = (r, 0)$ *robustly* w.r.t. any unknown static friction $\bar{F}_s$, for any constant r, and (2) improves the settling time (transient performance), compared to a classical PID controller.

The presence of an integrator action in $\bar{u}$ is motivated by the fact that it is able to compensate for an *unknown* static friction $\bar{F}_s$, which is typically the case in motion applications, so that the controller can robustly deal with the Coulomb friction effect. Before presenting our proposed *reset* PID controller, we first introduce the *classical* PID controller generating $\bar{u}$ as

$$\bar{u} = -\bar{k}_p(z_1 - r) - \bar{k}_d z_2 - \bar{k}_i z_3, \quad \dot{z}_3 = z_1 - r, \tag{3}$$

where $\bar{k}_p$, $\bar{k}_d$, $\bar{k}_i > 0$ represent the proportional, derivative and integral gains, respectively. We apply then the following definitions to obtain mass-normalized system dynamics that favor clarity in the analysis of the upcoming sections:

$$k_p := \tfrac{\bar{k}_p}{m}, \quad k_d := \tfrac{\bar{k}_d + \gamma}{m}, \quad k_i := \tfrac{\bar{k}_i}{m}, \quad F_s := \tfrac{\bar{F}_s}{m}. \tag{4}$$

By using (4), the resulting mass-normalized, closed-loop dynamics given by (1)–(3) satisfy

$$\begin{aligned} \dot{z}_1 &= z_2, \\ \dot{z}_2 &\in -F_s \operatorname{Sign}(z_2) - k_p(z_1 - r) - k_d z_2 - k_i z_3, \\ \dot{z}_3 &= z_1 - r, \end{aligned} \tag{5}$$

with the state vector $z = (z_1, z_2, z_3) \in \mathbb{R}^3$. We select the (normalized) controller gains such that the next assumption is satisfied.

Assumption 1. The control parameters k_p, k_d, k_i satisfy $k_i > 0$, $k_p > 0$, $k_p k_d > k_i$.

When $F_s = 0$ (a special, *linear* case of our setting), this assumption is equivalent, by the Routh–Hurwitz stability criterion, to ensuring global exponential stability of the equilibrium $z_1 = r$, $z_2 = z_3 = 0$ through a stabilizing PID controller. Assumption 1 is hence not restrictive.

In Bisoffi et al. (2018), it is proven that the set of equilibria

$$\mathcal{A} := \{z = (r, 0, z_3) \mid |z_3| \le F_s/k_i\} \tag{6}$$

of (5) is globally asymptotically stable under Assumption 1. However, the PID-controlled system (5) typically results in long settling times due to the depletion and refilling of the integral buffer that is required to overcome the static friction F_s upon overshoot, resulting in a change of sign of the integrator state of the PID controller (as illustrated in Beerens et al. (2018, §V and Fig. 3)). This process is generally slow and takes increasingly more time with a decreasing position error, resulting in long periods of stick and thus a poor transient performance in the sense of settling times. Note that the system is said to be in a *stick* or *slip* phase when the state belongs respectively to the sets

$$\mathcal{E}_{\text{stick}} := \{z \in \mathbb{R}^3 \,|\, z_2 = 0, |k_i z_3 + k_p(z_1 - r)| \le F_s\}, \tag{7a}$$

$$\mathcal{E}_{\text{slip}} := \mathbb{R}^3 \backslash \mathcal{E}_{\text{stick}}. \tag{7b}$$

In this paper, we propose a novel *reset* PID control scheme to solve Problem 1. In particular, the objective of the proposed reset integral controller is to obtain a significantly faster settling time (i.e., the time for the position error to reach and remain in a specified accuracy band) compared to the *classical* PID design in (3), resulting in (5). To this end, we replace the integrator in the PID controller (3) with a reset integrator. The key mechanism behind the reset integrator is that a large part of the time-consuming depletion and refilling process of the integrator buffer (needed to overcome the static friction) is circumvented, whenever the system overshoots the setpoint. The reset in (8c) below ensures that the control force after a reset points in the direction of the setpoint, as close as possible to the (unknown) static friction value. This results in the following reset PID controller:

$$\bar{u} = -\bar{k}_p(z_1 - r) - \bar{k}_d z_2 - \bar{k}_i z_3, \tag{8a}$$

$$\dot{z}_3 = z_1 - r, \tag{8b}$$

$$z_3^+ = -\alpha z_3 - (1 + \alpha)\tfrac{k_p}{k_i}(z_1 - r), \tag{8c}$$

where z_3^+ denotes the updated value of z_3 upon a reset, occurring only when the conditions (8e) below are satisfied. The design parameter $\alpha \in [0, 1]$ enables the reset to be scaled, and its role is elaborated further in Section 5. Position z_1 and velocity z_2 do not change at a reset:

$$z_1^+ = z_1, \quad z_2^+ = z_2. \tag{8d}$$

The integrator should be reset (as in (8e) below) whenever (*i*) the system overshoots the setpoint, and (*ii*) it enters a stick phase. Resetting the integrator when the system is in stick minimizes the risk of exciting high-frequency system dynamics because the discontinuity associated with the controller reset is compensated by the set-valued friction. See Beerens et al. (2018, §V) for an elaborate analysis of this fact. Intuitively speaking, condition (*i*) is met when the position error and the proportional–integral (PI) component of the controller have opposite sign. The satisfaction of condition (*ii*) requires the detection of zero velocity, which may be hard in practice due to measurement noise. Although robust zero-velocity detection mechanisms exist, we choose to evaluate the product of the PI control force and the velocity signal in order to robustly detect hitting zero velocity (see also Remark 1 below). Finally, we introduce a design parameter $\varepsilon > 0$ whose purpose is to avoid Zeno behavior (Goebel et al., 2012, pp. 28–29). This discussion motivates the controller reset conditions:

$$\begin{aligned} &k_i(z_1 - r)\left(k_p(z_1 - r) + k_i z_3\right) \le 0 \\ &\quad \wedge -z_2(k_p(z_1 - r) + k_i z_3) \le 0 \\ &\quad \wedge |k_p k_i (z_1 - r)^2 + k_i^2 (z_1 - r) z_3| \ge \varepsilon \end{aligned} \tag{8e}$$

In Section 3, we further elaborate on the reset map in (8c), the reset conditions in (8e), and the role of ε by showing that the reset conditions correspond indeed to (robust) detection of overshoot and stick (see (7a)). Moreover, we show in Section 4 that the reset map in (8c) preserves global asymptotic stability of the set of equilibria (6) for $\alpha \in [0, 1]$ and $\varepsilon > 0$ (note that in Beerens et al. (2018) only the case $\alpha = 1$ was considered). Summarizing, the resulting closed-loop system with the proposed reset PID controller is given by (5), (8c)–(8e).

3. Hybrid system formulation

In this section, we rewrite the closed-loop reset control system (5), (8c)–(8e) in the hybrid systems formalism of Goebel et al. (2012) to elaborate on the design of the proposed reset law. Furthermore, the derived hybrid system is used later for the stability analysis of Section 4.

Let us start with a useful state transformation, which allows for a simpler description of the system, transforms any constant setpoint r to the setpoint 0, and facilitates the construction of a Lyapunov-like function for the stability analysis in Section 4. Following Bisoffi et al. (2018), this state transformation is

$$x := \begin{bmatrix} \sigma \\ \phi \\ v \end{bmatrix} := \begin{bmatrix} -k_i(z_1 - r) \\ -k_p(z_1 - r) - k_i z_3 \\ z_2 \end{bmatrix}, \tag{9}$$

where σ is a generalized position error, ϕ is the controller state encompassing the proportional and integral control actions, and v is the velocity of the mass. The state transformation in (9) rewrites the stick set in (7a) as

$$\mathcal{E}_{\text{stick}} = \{x \in \mathbb{R}^3 \mid v = 0, \ |\phi| \le F_s\}. \tag{10}$$

The generalized controller state ϕ represents all the nonzero components of the control action at zero velocity (that is, the proportional and integral terms), and the size of ϕ compared to the static friction F_s at $v = 0$ determines then whether the system resides in a stick phase or not, see (10).

With the state transformation (9), we rewrite the closed-loop dynamics (5) with the reset law (8c)–(8d) in the hybrid formalism of Goebel et al. (2012) as in (11). The reset law (8c)–(8d) expressed in the state x simply yields a scaled sign change of ϕ when the reset criteria are met.

$$\dot{x} \in F(x) := \begin{bmatrix} -k_i v \\ \sigma - k_p v \\ \phi - k_d v - F_s \operatorname{Sign}(v) \end{bmatrix}, \qquad x \in \mathcal{C}, \tag{11a}$$

$$x^+ = g(x) := \begin{bmatrix} \sigma & -\alpha\phi & v \end{bmatrix}^\top, \qquad x \in \mathcal{D}, \tag{11b}$$

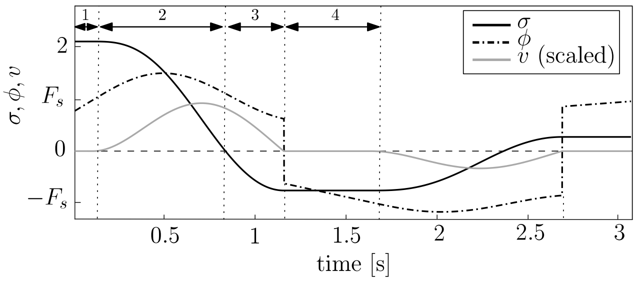

Fig. 1. Possible state evolution with the proposed controller. The integrator resets via a sign change of ϕ are clearly visible.

where F and g are the flow and jump map, respectively. Using (9), the reset conditions in (8e) transform into

$$\mathcal{D} := \left\{x \in \mathbb{R}^3 \mid \phi\sigma \le 0,\ \phi v \le 0,\ |\phi\sigma| \ge \varepsilon\right\}. \tag{11c}$$

Finally, the flow set is given by

$$\mathcal{C} := \overline{\mathbb{R}^3 \setminus \mathcal{D}}. \tag{11d}$$

Let us elaborate on the rationale behind the design of the jump set $\mathcal{D}$ using Fig. 1, which is an example of a response that could be obtained with the proposed reset controller in the coordinates x. Recall that we want the integrator to be reset (i.e., a jump is desired in the hybrid formulation in (11)) when the system satisfies the following two conditions at the same time: (1) it enters a stick phase, and (2) the position overshoots the setpoint. Namely, a reset in such conditions greatly reduces the time needed for the depletion and refilling of the integrator buffer, and consequently the stick duration. This is the key mechanism to improve the transient performance in terms of settling using reset control and contributes to solving the second item of Problem 1. Let us now discuss Fig. 1.

(1) Suppose the solution has initial condition $\sigma > 0$, $\phi > 0$, and $v = 0$, and starts in a stick phase (time interval 1 in Fig. 1). Due to the dynamics of the integrator, $\phi > F_s$ is eventually reached, which results in a slip phase (intervals 2 and 3 in Fig. 1). The solution enters a stick phase again (interval 4 in Fig. 1) when $v = 0$ is reached and the controller state ϕ satisfies $0 < \phi < F_s$. At this point, the condition $\phi v \le 0$ is satisfied.

A reset should not take place if the solution enters a stick phase *without* the occurrence of an overshoot, due to, e.g., different initial conditions, tuning, or friction characteristics. In such situations the solution still enters a stick phase and item (1) is satisfied. For this reason, we require the additional condition $\phi\sigma \le 0$ in the jump set $\mathcal{D}$ in (11c) as we explain now.

(2) Before an overshoot of the setpoint (interval 2 in Fig. 1), we have positive σ and ϕ, and thus $\phi\sigma > 0$. After an overshoot (interval 3 in Fig. 1), σ changes sign so that $\phi\sigma \le 0$. Along with item (1), we conclude that $\phi\sigma \le 0$ in $\mathcal{D}$ enforces indeed that a reset only takes place when the solution enters a stick phase *after* an overshoot.

Finally, the condition $|\phi\sigma| \ge \varepsilon$ in (11c), for some design parameter $\varepsilon > 0$, prevents a jump when σ or ϕ is zero, so that Zeno behavior is avoided. We will transform this condition into a more intuitive one in Section 5 (while leaving intact the stability results presented in the next section), where we provide tuning guidelines for ε as well.

Remark 1. To detect the stick phase, the criterion $\phi v \le 0$ is chosen in the jump set $\mathcal{D}$ in (11c) rather than just $v = 0$, since the latter is hard to check in practice due to velocity measurement noise. Although measurement noise around zero velocity may also render the product ϕv sign indefinite due to chattering in the sign of v, the additional condition $\phi\sigma \le 0$ in $\mathcal{D}$ prevents the system from experiencing undesired consecutive jumps. Indeed, after the first reset, the jump map (11b) ensures that $\phi\sigma > 0$, thus $x^+ \notin \mathcal{D}$. In this way the design of the reset condition warrants robustness against measurement noise in v.

Remark 2. The jump set $\mathcal{D}$ is expressed in (11c) in terms of x. The states ϕ and σ are not measurable in the case of an unknown mass m, as one can see from (9) and (4). The same observation clearly holds for the condition in (8e). However, even for an unknown mass m, we can define from (9) and (4) the measurable states

$$\varsigma := m\sigma = -\bar{k}_i(z_1 - r), \tag{12a}$$

$$\varphi := m\phi = -\bar{k}_p(z_1 - r) - \bar{k}_i z_3. \tag{12b}$$

This leads to jump conditions that can be checked based on the measurable states ς and φ, in which m does not appear. Note that for some $\epsilon > 0$, $|\varphi\varsigma| \ge \epsilon$ can replace $|\phi\sigma| \ge \varepsilon$ since ε is a design parameter.

4. Stability analysis

The set of equilibria (6) can be rewritten by the state transformation in (9) as

$$\mathcal{A} = \{x \in \mathbb{R}^3 \mid \sigma = v = 0,\ |\phi| \le F_s\}. \tag{13}$$

In this section, we show that (13) is globally asymptotically stable for (11), solving item (1) of Problem 1, as formalized by the next theorem.

Theorem 1. *Under Assumption 1, for each $\alpha \in [0, 1]$ and $\varepsilon > 0$, $\mathcal{A}$ in (13) is globally asymptotically stable for the hybrid dynamics (11).*

The remainder of this section is devoted to the proof of Theorem 1. In particular, we establish in Lemma 4 that $\mathcal{A}$ is globally attractive, and in Lemma 6 that $\mathcal{A}$ is Lyapunov stable for (11). The proof builds upon the results in Bisoffi et al. (2018), but is significantly challenged by the addition of the reset controller that gives rise to a *hybrid* (and no longer purely continuous-time) closed-loop system.

Consider the discontinuous Lyapunov-like function $V : \mathbb{R}^3 \to \mathbb{R}$ proposed in Bisoffi et al. (2018) and defined as

$$V(x) := \begin{bmatrix}\sigma \\ v\end{bmatrix}^\top \begin{bmatrix}\frac{k_d}{k_i} & -1 \\ -1 & k_p\end{bmatrix} \begin{bmatrix}\sigma \\ v\end{bmatrix} + \min_{F \in F_s \operatorname{Sign}(v)} (\phi - F)^2. \tag{14}$$

We start by providing some properties of solutions while flowing, as in Lemma 1 below. To this end, we note that (11a) (and function (14)) suggests that during flow there are three relevant affine subsystems corresponding to the system being in slip with nonnegative or nonpositive velocity, and being in stick (cf. (7b) and (10)). With the definitions

$$A := \begin{bmatrix} 0 & 0 & -k_i \\ 1 & 0 & -k_p \\ 0 & 1 & -k_d \end{bmatrix},\ b := \begin{bmatrix} 0 \\ 0 \\ F_s \end{bmatrix},\ P := \begin{bmatrix} \frac{k_d}{k_i} & 0 & -1 \\ 0 & 1 & 0 \\ -1 & 0 & k_p \end{bmatrix}, \tag{15}$$

these three subsystems are defined as

$$\dot{\xi} = f_1(\xi) := A\xi - b, \qquad \xi(t_0) = \xi_1, \tag{16a}$$

$$\dot{\xi} = f_0(\xi) := \begin{bmatrix} 0 & 0 & 0 \\ 1 & 0 & 0 \\ 0 & 0 & 0 \end{bmatrix}\xi, \qquad \xi(t_0) = \xi_0, \tag{16b}$$

$$\dot{\xi} = f_{-1}(\xi) := A\xi + b, \qquad \xi(t_0) = \xi_{-1}. \tag{16c}$$

For $\xi = (\xi_\sigma, \xi_\phi, \xi_v) \in \mathbb{R}^3$ and $|\xi|_P^2 := \xi^T P \xi$, define also

$$V_1(\xi) := \left|\begin{bmatrix} \xi_\sigma \\ \xi_\phi - F_s \\ \xi_v \end{bmatrix}\right|_P^2,\ V_0(\xi) := \left|\begin{bmatrix} \xi_\sigma \\ 0 \\ 0 \end{bmatrix}\right|_P^2,\ V_{-1}(\xi) := \left|\begin{bmatrix} \xi_\sigma \\ \xi_\phi + F_s \\ \xi_v \end{bmatrix}\right|_P^2. \tag{16d}$$

Table 1
Selection of k in item (ii) of Lemma 1 for each possible initial condition.

Initial condition $(\bar\sigma, \bar\phi, \bar v) := x(t, j)$	k
$(\bar v > 0) \vee (\bar v = 0 \wedge \bar\phi > F_s) \vee (\bar v = 0 \wedge \bar\phi = F_s \wedge \bar\sigma > 0)$	1
$(\bar v = 0 \wedge \bar\phi = F_s \wedge \bar\sigma \le 0)$ $\vee (\bar v = 0 \wedge \lvert\bar\phi\rvert < F_s) \vee (\bar v = 0 \wedge \bar\phi = -F_s \wedge \bar\sigma \ge 0)$	0
$(\bar v = 0 \wedge \bar\phi = -F_s \wedge \bar\sigma < 0) \vee (\bar v = 0 \wedge \bar\phi < -F_s) \vee (\bar v < 0)$	−1

With these definitions in place, we can state Lemma 1. Its item (i) asserts that flowing solutions to (11) are unique (in spite of the differential inclusion in (11a)), whereas its item (ii) relates such a (unique) flowing solution with the solution of one of the subsystems (16a)–(16c). The solution x to a hybrid dynamical system and its hybrid time domain dom x are defined respectively in Goebel et al. (2012, Def. 2.6) and Goebel et al. (2012, Def. 2.3).

Lemma 1. *For each solution x to (11), each interval $I^j := \{t : (t, j) \in \operatorname{dom} x\} =: [t_j, t_{j+1}]$ with nonempty interior, and for all $t \in (t_j, t_{j+1})$,*

(i) if $\hat x = (\hat\sigma, \hat\phi, \hat v)$ is a solution to (11) on $[t, t') \times \{j\}$ with $t < t' \le t_{j+1}$ and $\hat x(t, j) = x(t, j)$, then $\hat x$ coincides with x on $[t, t') \times \{j\}$;

(ii) one can select $k \in \{-1, 0, 1\}$ and $T > 0$ such that the unique solution $\xi = (\xi_\sigma, \xi_\phi, \xi_v)$ to (16) with initial condition $\xi_k = x(t, j)$ and $t_0 = t$, coincides on $[t, t + T]$ with $x(\cdot, j)$ and, additionally, V in (14) and V_k in (16d) evaluated along ξ satisfy for all $\tau \in [t, t + T]$:

$$V(\xi(\tau)) = V_k(\xi(\tau)) \text{ and } \tag{17a}$$

$$\tfrac{d}{d\tau} V_k(\xi(\tau)) \le -c\lvert\xi_v(\tau)\rvert^2, \tag{17b}$$

with

$$c := 2(k_p k_d - k_i) > 0. \tag{18}$$

Proof. The proof of Lemma 1 is based on the proofs of Bisoffi et al. (2018, Lemma 1 and Claim 1). Note that $c > 0$ in (18) by Assumption 1.

Item (i). The proof of this item is carried out analogously to Bisoffi et al. (2018, Proof of Lemma 1) for each one of the nonempty intervals $[t, t') \times \{j\}$.

Item (ii). For each possible initial condition $(\bar\sigma, \bar\phi, \bar v) := x(t, j)$, k in item (ii) is selected based on Table 1. The proof is then carried out analogously to Bisoffi et al. (2018, Appendix A) by substituting into (11) the solution ξ to the kth affine subsystem $\dot\xi = f_k(\xi)$ among (16a)–(16c) and verifying that (11) holds for ξ. Moreover, by evaluating V and V_k along the same ξ, and finally by differentiating $V_k(\xi(\cdot))$ w.r.t. time, we obtain (17). □

Exploiting Lemma 1, we are ready to present the properties of V in (14) in Lemma 2 below. We will use fact that the distance of a point $x \in \mathbb{R}^3$ to the attractor $\mathcal{A}$ in (13) is obtained from the definition as

$$\lvert x\rvert_{\mathcal{A}}^2 := \Big(\inf_{y\in\mathcal{A}} \lvert x - y\rvert\Big)^2 = \sigma^2 + v^2 + \mathrm{dz}_{F_s}(\phi)^2, \tag{19}$$

by separating the cases $\phi < -F_s$, $\lvert\phi\rvert \le F_s$, $\phi > F_s$.

Lemma 2. *V in (14) is lower semicontinuous (lsc) and enjoys the following properties:*

(1) $V(x) = 0$ for all $x \in \mathcal{A}$ and there exists $c_1 > 0$ such that $c_1\lvert x\rvert_{\mathcal{A}}^2 \le V(x)$ for all $x \in \mathbb{R}^3$.

(2) Given c in (18), each solution x satisfies

$$V(x(t_2, j)) - V(x(t_1, j)) \le -c \int_{t_1}^{t_2} v(t, j)^2 dt \tag{20}$$

for all t_1, t_2 in each (flow) interval $I^j := \{t : (t, j) \in \operatorname{dom} x\}$ with nonempty interior, and $t_1 \le t_2$.

(3) For all $x \in \mathcal{D}$ in (11c) it holds that

$$V(g(x)) - V(x) \le 0. \tag{21}$$

Proof. Based on Assumption 1, the proof of V being lsc and of item (1) is identical to Bisoffi et al. (2018, Proof of Lemma 2).

Item (2). To prove this item, we use (Hagood & Thomson, 2006, Thm. 9) with the variant in Hagood and Thomson (2006, Sec. 5 (point a.)), as in the following Fact 1. The statement is specialized for an integrable function l, so that the standard integral can replace the upper integral in Hagood and Thomson (2006, Thm. 9), as noted after Hagood and Thomson (2006, Def. 8).

Fact 1 (*Hagood & Thomson, 2006*)**.** *Given $t_2 > t_1 \ge 0$, suppose that h is lower semicontinuous and that l is locally integrable in $[t_1, t_2]$. If $D_+h(\tau) \le l(\tau)$ for all $\tau \in [t_1, t_2]$, then $h(t_2) - h(t_1) \le \int_{t_1}^{t_2} l(\tau)d\tau$.*

By the preliminary Lemma 1, (20) in item (2) is a mere application of Fact 1 for $h(\cdot) = V(x(\cdot, j))$ and $l(\cdot) = -cv(\cdot, j)^2$ where $x = (\sigma, \phi, v)$ is a solution to (11). So, we need to check that the assumptions of Fact 1 are verified. We already established above that $V(\cdot)$ is lsc. Solutions x to (11) are such that for each $j \in \mathbb{Z}_{\ge 0}$, $t \mapsto x(t, j)$ is locally absolutely continuous by Goebel et al. (2012, Def. 2.4 and 2.6). Then, because the composition of a lsc and a continuous function is lsc (Rockafellar & Wets, 2009, Exercise 1.40), the Lyapunov-like function V in (14) evaluated along the flow portion of a solution to (11) is lsc in t. Because of the local absolute continuity of flowing portions of solutions, $-cv(\cdot, j)^2$ is locally integrable.

Finally, it was proven in item (ii) of Lemma 1 that on I^j, the solution x to (11) coincides with the solution ξ to one of the three affine systems in (16) (numbered k) on $[t, t+T]$. Moreover, that same item states that $V(\xi(\cdot))$ coincides in $[t, t + T]$ with the function $V_k(\xi(\cdot))$ in (17), which is differentiable, hence $V(x(\cdot, j))$ is at least differentiable from the right at t and the lower right Dini derivative coincides with the right derivative. In particular, we established in (17) that this right derivative is upper bounded by $-cv(\cdot, j)^2$.

Item (3). For all $x \in \mathcal{D}$ in (11c), $V(g(x)) - V(x) = \min_{F\in F_s \operatorname{Sign}(v)}(-\alpha\phi - F)^2 - \min_{F\in F_s \operatorname{Sign}(v)}(\phi - F)^2$ where for each v, the set $F_s \operatorname{Sign}(v)$ is compact. Then,

$$V(g(x)) - V(x) = \begin{cases} (\alpha^2 - 1)\phi^2 + 2(\alpha + 1)\phi F_s \operatorname{sign}(v), & \text{if } v \ne 0, \\ \big(\alpha \mathrm{dz}_{\frac{F_s}{\alpha}}(\phi)\big)^2 - \big(\mathrm{dz}_{F_s}(\phi)\big)^2, & \text{if } v = 0, \end{cases} \tag{22}$$

by evaluating the different cases for v and ϕ. The inequality in (21) follows from (22) since $0 \le \alpha \le 1$ and $\phi v \le 0$ in the jump set $\mathcal{D}$. □

The properties of V in Lemma 2 imply that maximal solutions are complete (Goebel et al., 2012, §2.3), as per the next lemma.

Lemma 3. *For each initial condition $\bar x \in \mathbb{R}^3$, each maximal solution x to (11) with $x(0, 0) = \bar x$ is complete.*

Proof. The proof is based on Goebel et al. (2012, Prop. 6.10), which can be applied since (11) satisfies the so-called hybrid basic conditions (Goebel et al., 2012, Ass. 6.5). Condition *(VC)* of Goebel et al. (2012, Prop. 6.10) holds for every $\xi \in \mathcal{C}\backslash\mathcal{D}$, otherwise we would contradict completeness in Bisoffi et al. (2018, Lem. 1). Therefore, each solution x satisfies exactly one of Goebel et al. (2012, Prop. 6.10, *(a)*–*(c)*). Note that (20) and (21) imply together that

$$V(x(t, j)) \le V(x(0, 0)) \tag{23}$$

for each $(t,j) \in \operatorname{dom} x$. If Goebel et al. (2012, Prop. 6.10, *(b)*) is verified (that is, $\lim_{t\to\sup_t \operatorname{dom} x} |x(t, \sup_j \operatorname{dom} x)| = +\infty$), then also V grows unbounded because of the lower bound of V in Item (1) of Lemma 2. But this is a contradiction of (23), so we can exclude (Goebel et al., 2012, Prop. 6.10, *(b)*) for each solution. Also (Goebel et al., 2012, Prop. 6.10, *(c)*) can be excluded since $\mathcal{C}\cup\mathcal{D}$ is $\mathbb{R}^3$ in (11). Then only (Goebel et al., 2012, Prop. 6.10, *(a)*) remains, i.e., each solution x is complete. $\square$

We can now prove global attractivity of $\mathcal{A}$ in (13) through a meagre-limpsup invariance principle (Goebel et al., 2012, Thm. 8.11) in the next lemma.

Lemma 4. *The set of equilibria $\mathcal{A}$ in (13) is globally attractive for dynamics (11).*

Proof. Goebel et al. (2012, Thm. 8.11) is applicable because (Goebel et al., 2012, Ass. 6.5) is satisfied by (11). Note that, since each maximal solution x to (11) is complete by Lemma 3, the conclusions of Goebel et al. (2012, Thm. 8.11) will hold for each maximal solution x once we verify that each such x satisfies the meagre-limsup conditions *(a)*–*(b)* below. More specifically, introduce the continuous functions $x \mapsto \ell_c(x) := v^2$ and $x \mapsto \ell_d(x) := 1$. Then, Goebel et al. (2012, Thm. 8.11) holds if:

(*a*) if $\sup_t \operatorname{dom} x = \infty$, then $t \mapsto \ell_c(x(t, j(t)))$ is weakly meagre (as defined in Goebel et al. (2012, p. 178)), where $j(t) := \min_{(t,j)\in\operatorname{dom} x} j$;

(*b*) for each maximal solution x^* to (11), if $(t, j-1), (t, j), (t, j+1) \in \operatorname{dom} x^*$, then $\ell_d(x^*(t, j)) = 0$.

Let us check condition (*a*). Lemma 2 (items 2–3) implies, for each solution x and a generic $(t,j) \in \operatorname{dom} x$, that $V(x(t,j)) - V(x(0,0)) \le -c\int_0^t v(\tau, j(\tau))^2 d\tau$, by splitting into flow intervals and jumps. We then have $\int_0^t \ell_c(x(\tau, j(\tau)))d\tau \le \frac{V(x(0,0))-V(x(t,j))}{c} \le \frac{V(x(0,0))}{c}$ by Lemma 2 (item 1). By letting $t \to +\infty$, this means that $t \mapsto \ell_c(x(t, j(t)))$ is absolutely integrable on $\mathbb{R}_{\ge 0}$ and is hence weakly meagre (see Goebel et al., 2012, p. 178).

Let us check condition (*b*). For all maximal solutions x^* to (11), there are no $(t, j-1), (t, j), (t, j+1) \in \operatorname{dom} x^*$ since each x^* cannot exhibit two or more consecutive jumps (by the definitions of g and $\mathcal{D}$, if both $(t, j-1)$ and $(t,j) \in \operatorname{dom} x^*$, then $x^*(t, j-1) \in \mathcal{D}$ and $x^*(t,j) \in \mathcal{C}\backslash\mathcal{D}$). So, condition (*b*) is (vacuously) satisfied.

Since (*a*) and (*b*) above hold, then Goebel et al. (2012, Thm. 8.11) concludes that for each solution x, $\Omega(x) \subset \{\chi \in \overline{\operatorname{rge}}\, x : v = 0\}$, where $\Omega(x)$ is the ω-limit set of solution x (Goebel et al., 2012, Def. 6.17) and $\overline{\operatorname{rge}}\, x$ denotes the closure of the range of x. Due to the properties of $\Omega(x)$ in Goebel et al. (2012, Prop. 6.21), its weak invariance implies that for each complete solution x, $\Omega(x)$ does not contain points where $\sigma \neq 0$ or $|\phi| > F_s$, because from these points all complete solutions eventually exhibit a nonzero velocity component. As a consequence, $\Omega(x) \subset \mathcal{A}$ for each complete solution x, which implies by Goebel et al. (2012, Prop. 6.21) that all complete solutions converge to $\mathcal{A}$, i.e., global attractivity of $\mathcal{A}$. $\square$

Finally, we now turn to proving stability of $\mathcal{A}$ in (13). As in Bisoffi et al. (2018), we need the auxiliary function

$$\hat{V}(x) := \tfrac{1}{2}k_1\sigma^2 + \tfrac{1}{2}k_2\big(\mathrm{dz}_{F_s}(\phi)\big)^2 + k_3|\sigma||v| + \tfrac{1}{2}k_4 v^2, \tag{24}$$

in order to prove stability through bound (26), in spite of the discontinuity of V in (14). Indeed, because of such discontinuity at points in the attractor $\mathcal{A}$, an upper bound of the type $c_2|x|^2_{\mathcal{A}}$ for $V(x)$ does not hold in $\mathbb{R}^3$, unlike the lower bound in Lemma 2 (item 1), and stability of $\mathcal{A}$ cannot be concluded directly from V. However, such lower and upper bounds, together with suitable growth bounds along solutions, can be established for V and $\hat{V}$, respectively, in the following partition of the state space $R := \{x \mid v(\phi - \operatorname{sign}(v)F_s) \ge 0\}$ and $\hat{R} := \mathbb{R}^3\backslash R$, as characterized in the next lemma.

Lemma 5. *For suitable positive scalars k_1, k_2, k_3, k_4 in (24), there exist positive scalars $c_1, c_2, \hat{c}_1, \hat{c}_2$ such that*

$$c_1|x|^2_{\mathcal{A}} \le V(x) \le c_2|x|^2_{\mathcal{A}}, \qquad \forall x \in R, \tag{25a}$$

$$\hat{c}_1|x|^2_{\mathcal{A}} \le \hat{V}(x) \le \hat{c}_2|x|^2_{\mathcal{A}}, \qquad \forall x \in \mathbb{R}^3, \tag{25b}$$

$$\hat{V}^\circ(x) := \max_{\mathfrak{v}\in\partial\hat{V}(x),\, \mathfrak{f}\in F(x)} \langle \mathfrak{v}, \mathfrak{f}\rangle \le 0, \qquad \forall x \in \hat{R}, \tag{25c}$$

$$\hat{V}(g(x)) - \hat{V}(x) \le 0 \qquad \forall x \in \hat{R}, \tag{25d}$$

where $\partial\hat{V}(x)$ denotes the generalized gradient of $\hat{V}$ at x as in Clarke (1990, §1.2), F is as in (11a), and g is as in (11b).

Proof. Eqs. (25a)–(25b) are proved analogously to Bisoffi et al. (2018, (19a)-(19b)). This is also true for (25c), since the flow map F is the same as well. Finally, (25d) holds since $\big(\mathrm{dz}_{F_s}(-\alpha\phi)\big)^2 \le \big(\mathrm{dz}_{F_s}(\phi)\big)^2$ for $\alpha \in [0, 1]$. $\square$

By composing the relations of Lemmas 5 and 2 for V and $\hat{V}$, the bound (26) of the next lemma can be obtained, which establishes (uniform global) stability (see Goebel et al., 2012, Def. 3.6) of $\mathcal{A}$ in (13).

Lemma 6. *Given the scalars $c_1, c_2, \hat{c}_1, \hat{c}_2$ in (25), each solution x to (11) satisfies*

$$|x(t,j)|_{\mathcal{A}} \le \sqrt{\frac{c_2\hat{c}_2}{c_1\hat{c}_1}}|x(0,0)|_{\mathcal{A}} \quad \forall (t,j) \in \operatorname{dom} x. \tag{26}$$

Proof. The proof is the natural extension to the hybrid case of the proof of Bisoffi et al. (2018, Proof of Item (2) of Prop. 1, Eq. (21)). In particular, one considers the two mutually exclusive *Case (i)* (i.e., $x(t,j) \notin R$ for all $(t,j) \in \operatorname{dom} x$) and *Case (ii)* (i.e., there exists $(\bar{t}, \bar{j}) \in \operatorname{dom} x$ such that $x(\bar{t}, \bar{j}) \in R$) and applies (25) and Lemma 2, items 1–3. $\square$

Remark 3. Since $\mathcal{A}$ is compact, and the hybrid system (11) satisfies the hybrid basic conditions (Goebel et al., 2012, Ass. 6.5), the stability and global attractivity results proven above imply *uniform* global asymptotic stability for (11) in terms of a class-$\mathcal{KL}$ estimate. They also imply global robust $\mathcal{KL}$ asymptotic stability of $\mathcal{A}$ for (11) (Goebel et al., 2012, Thm. 7.21) and semiglobal practical robust asymptotic stability of $\mathcal{A}$ (Goebel et al., 2012, Thm. 7.12 and Lemma 7.20).

5. Experimental case study

In this section, we demonstrate the working principle and the effectiveness of the proposed reset controller on an industrial high-precision positioning stage. The considered stage represents a sample manipulation stage of an electron microscope (Thermo Fisher Scientific). In particular, we show (1) the robust stability properties of the controller in the presence of unknown static friction and measurement noise, (2) that the transient performance is indeed improved w.r.t. the classical PID controller, as in item 2 of Problem 1, and (3) how the tuning of the reset controller affects performance.

5.1. Experimental setup

The experimental setup is presented in Fig. 2. The setup consists of a Maxon RE25 DC servo motor ① connected to a spindle

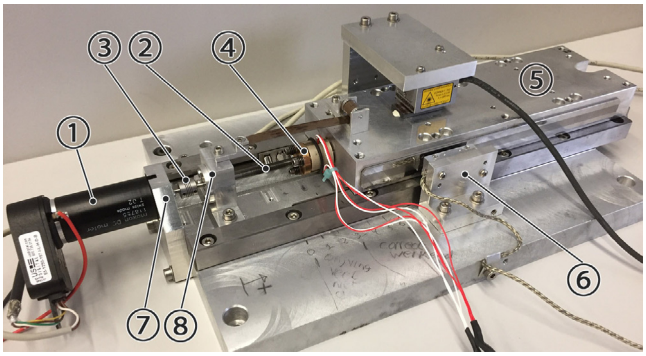

Fig. 2. Experimental setup of a nano-positioning motion stage.

② via a coupling ③ that is stiff in the rotational direction while being flexible in the translational direction. The spindle drives a nut ④, transforming the rotary motion of the spindle to a translational motion of the attached carriage ⑤, with a ratio of $7.96 \cdot 10^{-5}$ m/rad. The position of the carriage is measured by a linear Renishaw encoder ⑥ with a resolution of 1 nm (and peak noise level of 4 nm). The desired position accuracy to be achieved is 10 nm, as specified by the manufacturer.

For frequencies up to 200 Hz, the system dynamics can be well described by (1) for which Theorem 1 applies when interconnected with the reset PID controller. In this case, z_1 represents the position of the carriage. The mass $m = 172.6$ kg consists of the transformed inertia of the motor and the spindle (with an *equivalent* mass of 171 kg), and of the mass of the carriage (1.6 kg).

The friction force for Ψ in (1) is mainly induced by the bearings supporting the motor axis and the spindle (see ⑦ and ⑧ in Fig. 2), and by the contact between the spindle and the nut. Since the system is rigid and behaves as a single mass for frequencies up to 200 Hz, these friction forces can be summed up to provide a single net friction characteristic as Ψ in (1). For illustrative purposes *only*, the net friction characteristic is experimentally identified and visualized in Fig. 3. It can be observed that the setup shows dominantly static Coulomb friction with static friction values of 32.7 N and 33.1 N for positive and negative motions, respectively, indicating a small level of asymmetry in the friction characteristic. On the other hand, it also shows a small Stribeck effect. The Stribeck effect, however, is insignificant as compared to the static friction, and does not require an additional compensation term in $\bar{u}$. As we will show below, the closed-loop with a (reset) PID controller results in asymptotic stability of the position setpoint, instead of hunting limit cycling (which may occur in the presence of a more pronounced Stribeck effect). This indicates that the considered system controlled by either the classical PID controller or the proposed reset controller has some robustness to small Stribeck effects. We emphasize that we do not use any of this information on the friction characteristic in our controller.

5.2. Reset controller tuning

The purpose of the experimental case study is to demonstrate the transient performance benefits that can be obtained with the proposed reset controller, in terms of settling time, relative to the classical PID controller.

The PID controller gains $\bar{k}_p = 10^7$ N/m, $\bar{k}_d = 2 \cdot 10^3$ N $\cdot$ s/m, and $\bar{k}_i = 10^8$ N/(m $\cdot$ s) are obtained by well-known linear loop-shaping techniques often applied in industry. The proposed reset integrator does not require additional tuning constraints other

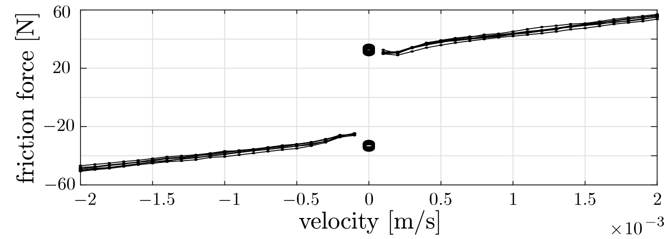

Fig. 3. Measured friction characteristic. The circles are static friction values obtained from breakaway experiments, and the solid lines connect velocity-dependent friction values for different initial positions.

than the "linear" stability conditions in Assumption 1 (indeed necessary for the special case $\bar{F}_s = 0$) that are equivalent to $\bar{k}_i > 0$, $\bar{k}_p > 0$, and $\frac{\bar{k}_p(\bar{k}_d+\gamma)}{m} > \bar{k}_i$. The latter holds since $\gamma > 0$ and the PID controller gains above satisfy $\frac{\bar{k}_p\bar{k}_d}{m} > \bar{k}_i$.

Let us now explain the role of the tuning parameter α. Most importantly, $\alpha \in [0, 1]$ directly affects the transient performance (a larger α leads to a faster convergence). Additionally, α accommodates the developments in Sections 2–4 for symmetric friction to possible asymmetries in the experimental friction characteristics. On the one hand, α closer to one yields a larger reset and a correspondingly shorter stick duration. Choosing α as large as possible is thus favorable for the transient performance improvement, and we will show the implications of the value for α on the transient performance in the next subsection. On the other hand, a smaller α results in a relaxed reset, hence a longer stick duration, which enhances robustness for frictional asymmetry as explained in detail in the next remark.

Remark 4. A smaller α yields robustness to an asymmetric friction characteristic. If the static friction value in the positive direction of motion is significantly larger than the static friction value in the negative direction of motion, the integrator has to build up a larger control force in the positive direction. It may then happen that *after the reset ensuing the beginning of a stick phase*, the value for the proportional and integral action exceeds the static friction value, resulting in an immediate escape from the stick phase and possibly unstable behavior. In other words, a controller reset (with α large) combined with asymmetric friction may lead to overcompensation, compromising the stability of the setpoint as analyzed in Putra et al. (2007).

The last tuning parameter ϵ comes from the criterion $|\varphi\varsigma| \geq \epsilon$ which replaces $|\phi\sigma| \geq \varepsilon$ in $\mathcal{D}$, as noted in Remark 2. The purpose of $|\varphi\varsigma| \geq \epsilon$ is to prevent a discrete jump when the measurable states ς or φ in (12) are zero, so that Zeno behavior is avoided. For practical implementation, we redefine this criterion to the more intuitive criteria $|\varsigma| \geq \eta_1$, $|\varphi| \geq \eta_2$, with $\eta_1, \eta_2 > 0$. We choose $\eta_1 = \bar{k}_i \cdot 10^{-8}$ m $= 1$ N/s, so that resets are inhibited when the carriage is within the desired position error accuracy band of 10^{-8} m (10 nm). Also, $\eta_2 = 1$ N $\cdot$ m $\cdot$ s is chosen so that resets are inhibited when φ is small, in order to avoid Zeno behavior. Using as in Remark 2 the measurable states ς and φ in (12), and the above alternative criteria, the jump set used for the experiments is then

$$\mathcal{D}^* := \{(\varsigma, \varphi, v) \in \mathbb{R}^3 \,|\, \varphi\varsigma \leq 0, \varphi v \leq 0, |\varsigma| \geq \eta_1, |\varphi| \geq \eta_2\}. \quad (27)$$

Note that ς is obtained from the position error measurement $z_1 - r$, and φ is obtained from both the position error measurement, and a recording of the integrator state z_3. We emphasize also that our main result in Theorem 1 and its proof hold unchanged if $\mathcal{D}^*$ replaces $\mathcal{D}$ in (11c).

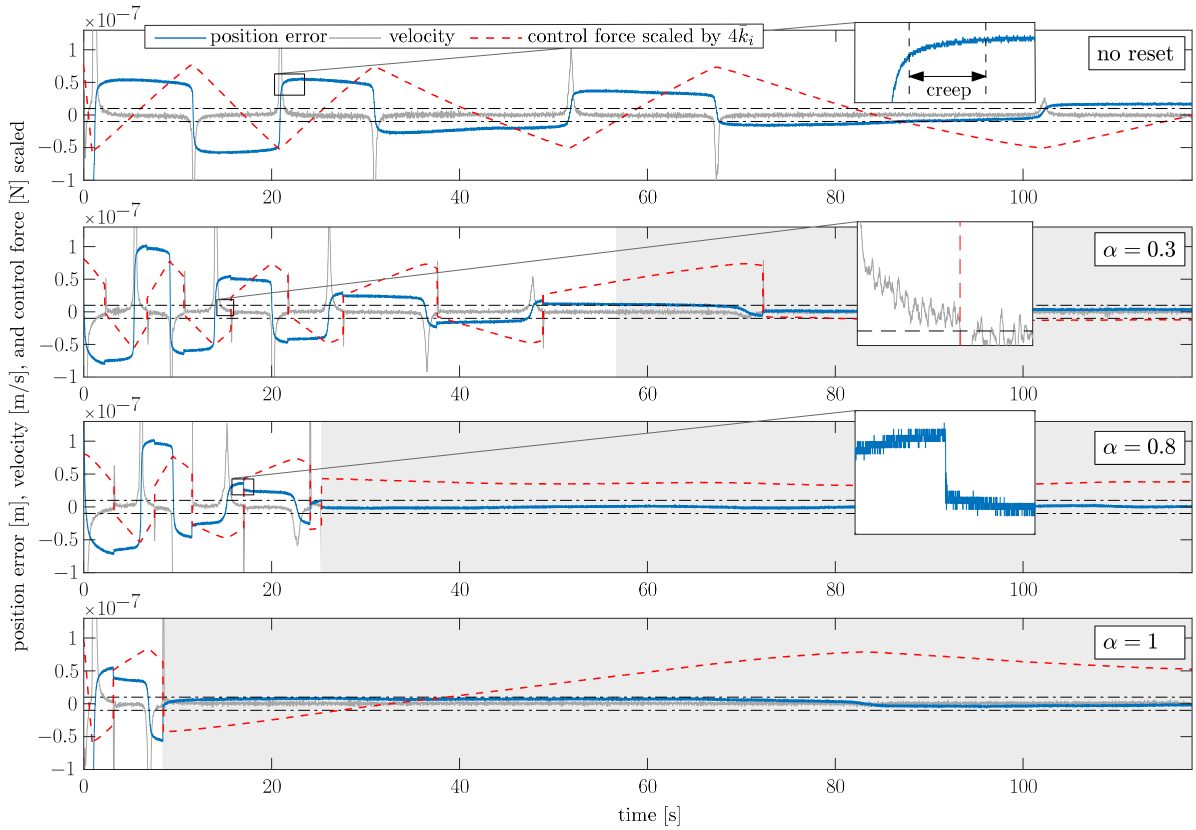

Fig. 4. Experimental results for various values of α. Blue: position error $z_1 - r$; gray: velocity; red: total control force scaled by $4\bar{k}_i$. The accuracy band of 10 nm is indicated by the black, dashed–dotted lines. The response resides within the desired accuracy from 56.7, 25.8, and 8.4 s onwards for α equal to 0.3, 0.8, and 1, respectively, as shown by the gray patches. (For interpretation of the references to color in this figure legend, the reader is referred to the web version of this article.)

5.3. Transient performance comparison

We now demonstrate the transient performance benefits of the proposed reset controller. According to standard operation of the nano-positioning stage in an electron microscope, a fourth-order reference trajectory is applied to the stage so that it moves by one millimeter in one second. After the trajectory has ended, the stage has a nonzero positioning error due to the presence of friction. This is the starting point of our window of interest during the experiments, and from this point on, the goal is to control the system towards a specified position error accuracy of 10 nm using the proposed reset controller. In particular, we show the *relative* improvement in terms of settling time (i.e., the required time for the position error to reach and remain in the error band of 10 nm), as compared to the underlying classical PID controller without resets.

The responses for the position error $z_1 - r$ and the corresponding scaled control force $\bar{u}/(4\bar{k}_i)$ are presented in Fig. 4 for the classical PID and the reset PID (with different values of α). All experiments are performed with the same initial conditions. Variations in the position errors and time instants of the initial stick phases between the presented responses are due to the fact that the friction characteristic is slightly different for each experiment, due to, e.g., small temperature changes as a result of continuous system operation. Since the setup operates on a very small position error regime, even minor changes in the friction may have a significant impact on the response. It can be observed in Fig. 4 that the application of the reset controller (see the three bottom plots for different values for α) results in shorter stick periods and hence decreased settling times, as compared to the classical PID controller (see the top plot). In particular, in the presented responses, the desired accuracy is achieved at respectively, 56.7, 25.3 and 8.4 s corresponding to values for α of 0.3, 0.8 and 1. Unlike the reset one, the classical PID controller (with the same controller gains), did not reach the desired accuracy within the maximal measurement window of 120 s.

We emphasize that false resets are not triggered due to the robust design of the jump set $\mathcal{D}$ (and its implementable version $\mathcal{D}^*$ in (27)) with respect to velocity measurement noise, as pointed out in Remark 1. The inset in the second subplot in Fig. 4 shows that indeed a reset is triggered as soon as the velocity hits zero (characterizing the start of a stick phase, as in (7a)). After the reset has occurred, the velocity signal keeps crossing zero during the stick phase, due to noise, but undesired multiple resets are prevented by the robust design of the reset conditions, in accordance with Remark 1.

5.4. Microscopic frictional effects

Due to the low position error levels in the operating conditions of the setup, microscopic frictional effects that are present in the friction characteristic are significant compared to the static friction effect in this particular application. The experimental results above show that the proposed control strategy also exhibits some robustness against these effects, although not formally analyzed in the presented stability result in Section 4.

Frictional creep

A controller reset occurs some time after the beginning of a macroscopic stick phase. This effect is caused by microscopic frictional creep (see, e.g., Armstrong-Hélouvry, 1992, Chap. 2) at the start of (and during) a macroscopic stick phase (see the inset in the first subplot of Fig. 4), thereby not allowing for a reset because of the nonzero velocity. Hitting $v = 0$ (so that $\varphi v \leq 0$ in $\mathcal{D}^*$ is satisfied) can be detected only when the microscopic creep stops. This is illustrated by the inset in the second subplot of Fig. 4, where we highlight the velocity signal during such a period of creep. A nonzero velocity is indeed observed during creep, and the controller is reset only as soon as the velocity signal hits zero (indicated by the black dashed horizontal line). The reset delay associated to creep allows then the integrator buffer to deplete, which, in turn, causes a milder reset. This milder reset further motivates us to choose $\alpha = 1$ despite the (minor) asymmetry in the friction characteristics (see Fig. 3).

Frictional stiffness effects

A second phenomenon caused by microscopic frictional effects is the small stick-to-stick jumps in the position error response upon resets, see the inset in the third subplot of Fig. 4. This phenomenon can be explained by the presence of stiffness-like characteristics in the friction, see e.g., Armstrong-Hélouvry et al. (1994, Sec. 2.1). To illustrate this, note that the magnitude of these stiffness-like effects can be estimated by dividing the difference in the control force associated with a controller reset, by the resulting change in position. This results in values between $8 \cdot 10^8$ and $7 \cdot 10^9$ N/m. Although these estimated stiffness coefficients are very large, the associated effect is significant due to the low position errors in the operating conditions. Note that the system still resides in the stick phase in macroscopic sense after the controller reset. In this case, these effects are not unfavorable, as they force the system towards the setpoint. On the other hand, the position error after such a jump is smaller, so that it takes more time for the integrator to compensate for the static friction.

6. Conclusions

We proposed a novel reset integrator control strategy for motion systems with friction that achieves, firstly, robust global asymptotic stability of the setpoint for unknown static friction and, secondly, improves transient performance by reducing the settling time. The reset conditions are designed so that a controller reset is correctly triggered despite measurement noise, and does not increase the risk of exciting high-frequency system dynamics. Global asymptotic stability of the setpoint is proven based on a generalized invariance principle for hybrid dynamical systems. An experimental case study on a high-precision positioning application shows the improved settling time when using the proposed reset controller, as compared to its classical PID counterpart.

Acknowledgment

The authors greatly acknowledge David Fresen for his assistance with the experimental part of this work.

References

Aangenent, W. H. T. M., Witvoet, G., Heemels, W. P. M. H., van de Molengraft, M. J. G., & Steinbuch, M. (2010). Performance analysis of reset control systems. *International Journal of Robust and Nonlinear Control*, *20*(11), 1213–1233.

Armstrong-Hélouvry, B. (1992). *Control of machines with friction*. New York: Spinger Science.

Armstrong-Hélouvry, B., Dupont, P., & Canudas de Wit, C. (1994). A survey of models, analysis tools and compensation methods for the control of machines with friction. *Automatica*, *30*(7), 1083–1138.

Bartolini, G., Pisano, A., Punta, E., & Usai, E. (2003). A survey of applications of second-order sliding mode control to mechanical systems. *International Journal of Control*, *76*, 875—892.

Beerens, R., Bisoffi, A., Zaccarian, L., Heemels, W. P. M. H., Nijmeijer, H., & van de Wouw, N. (2018). Hybrid PID control for transient performance improvement of motion systems with friction. In *Amer. control conference* (pp. 539–544).

Beerens, R., Nijmeijer, H., Heemels, W. P. M. H., & van de Wouw, N. (2017). Set-point control of motion systems with uncertain set-valued Stribeck friction. *IFAC PapersOnline*, *50*(1), 2965–2970.

Bisoffi, A., Da Lio, M., Teel, A. R., & Zaccarian, L. (2018). Global asymptotic stability of a PID control system with Coulomb friction. *IEEE Transactions on Automation Control*.

Clarke, F. H. (1990). *Optimization and nonsmooth analysis*. Philadelphia: SIAM.

Clegg, J. C. (1958). A nonlinear integrator for servomechanisms. *Transactions on American Institute of Electrical Engineers, Part II: Applications and Industry*, *77*(1), 41–42.

Deenen, D. A., Heertjes, M. F., Heemels, W. P. M. H., & Nijmeijer, H. (2017). Hybrid integrator design for enhanced tracking in motion control. In *Amer. control conference* (pp. 2863–2868).

El Rifai, K., & El Rifai, O. (2009). Design of hybrid resetting PID and lag controllers with application to motion control. In *Int. conf. adv. intell. mechatron.* (pp. 685–692).

Freidovich, L., Robertsson, A., Shiriaev, A., & Johansson, R. (2010). LuGre-model-based Friction compensation. *IEEE Transactions on Control Systems and Technology*, *18*(1), 194–200.

Goebel, R., Sanfelice, R. G., & Teel, A. R. (2012). *Hybrid dynamical systems*. Princeton: Princeton University Press.

Hagood, J. W., & Thomson, B. S. (2006). Recovering a function from a Dini derivative. *American Mathematical Monthly*, *113*(1), 34–46.

Hensen, R. H. A., van de Molengraft, M. J. G., & Steinbuch, M. (2003). Friction induced hunting limit cycles: A comparison between the LuGre and switch friction model. *Automatica*, *39*(12), 2131–2137.

Horowitz, I., & Rosenbaum, P. (1975). Non-linear design for cost of feedback reduction in systems with large parameter uncertainty. *International Journal of Control*, *21*(6), 977–1001.

Iannelli, L., Johansson, K. H., Jönsson, U. T., & Vasca, F. (2006). Averaging of nonsmooth systems using dither. *Automatica*, *42*(4), 669–676.

van Loon, S. J. L. M., Gruntjens, K. G. J., Heertjes, M. F., van de Wouw, N., & Heemels, W. P. M. H. (2017). Frequency-domain tools for stability analysis of reset control systems. *Automatica*, *82*, 101–108.

van Loon, S. J. L. M., Hunnekens, B. G. B., Heemels, W. P. M. H., van de Wouw, N., & Nijmeijer, H. (2016). Split-path nonlinear integral control for transient performance improvement. *Automatica*, *66*, 262–270.

Makkar, C., Hu, G., Sawyer, W. G., & Dixon, W. E. (2007). Lyapunov-based tracking control in the presence of uncertain nonlinear parameterizable friction. *IEEE Transactions on Automation Control*, *52*(10), 1988–1994.

Nešić, D., Teel, A. R., & Zaccarian, L. (2011). Stability and performance of SISO control systems with first-order reset elements. *IEEE T. Automat. Contr.*, *56*(11), 2567–2582.

Nešić, D., Zaccarian, L., & Teel, A. R. (2008). Stability properties of reset systems. *Automatica*, *44*, 2019–2026.

Orlov, Y., Santiesteban, R., & Aguilar, L. T. (2009). Impulsive control of a mechanical oscillator with friction. In *Amer. control conference* (pp. 3494–3499).

Putra, D., Nijmeijer, H., & van de Wouw, N. (2007). Analysis of undercompensation and overcompensation of friction in 1DOF mechanical systems. *Automatica*, *43*(8), 1387–1394.

Rockafellar, R. T., & Wets, R. J.-B. (2009). *Variational analysis*. Berlin Heidelberg: Springer Science & Business Media.

Thermo Fisher Scientific. https://www.fei.com/products/.

Thomsen, J. J. (1999). Using fast vibrations to quench friction-induced oscillations. *Journal of Sound and Vibration*, *228*(5), 1079–1102.

van de Wouw, N., & Leine, R. I. (2012). Robust impulsive control of motion systems with uncertain friction. *International Journal of Robust and Nonlinear Control*, *22*, 369–397.

Zhao, G., & Wang, J. (2016). On $\mathcal{L}_2$ gain performance improvement of linear systems with Lyapunov-based reset control. *Nonlinear Analysis. Hybrid Systems*, *21*, 105—117.

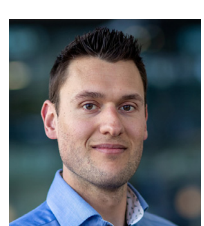

Ruud Beerens received the M.Sc. degree in mechanical engineering at Eindhoven University of Technology, The Netherlands, in 2015, where he is currently pursuing the Ph.D. degree in the Department of Mechanical Engineering. His current research focus is on nonlinear and hybrid control design for high-performance mechatronic systems.

Andrea Bisoffi received the M.Sc. degree in Automatic Control Engineering from Politecnico di Milano, Italy, in 2013 and the Ph.D. degree in Mechatronics from the University of Trento, Italy, in 2017. In 2015–2016 he was a visiting scholar in the Control Group at the University of Cambridge, UK. He is currently a postdoctoral researcher at KTH Royal Institute of Technology, Sweden. His current research interests include hybrid and nonlinear control systems, with applications to mechanical, automotive and robotic systems.

Luca Zaccarian received the Laurea and the Ph.D. degrees from the University of Roma Tor Vergata (Italy) in 1995 and 2000, respectively. He has been Assistant Professor in control engineering at the University of Roma, Tor Vergata (Italy), from 2000 to 2006 and then Associate Professor. Since 2011 he is Directeur de Recherche at the LAAS-CNRS, Toulouse (France) and since 2013 he holds a part-time associate professor position at the University of Trento, Italy. Luca Zaccarian's main research interests include analysis and design of nonlinear and hybrid control systems, modeling and control of mechatronic systems. He was a nominated member of the Board of Governors of the IEEE-CSS in 2014, where he is an elected member in 2017–2019. He was Student Activities Chair for the IEEE-CSS in 2015–2017 and is currently Associate Editor of Electronic Publications (Conference Information) for the IEEE-CSS. He was a recipient of the 2001 O. Hugo Schuck Best Paper Award given by the American Automatic Control Council. He is a fellow of the IEEE, class of 2016.

W.P.M.H. Heemels received the M.Sc. degree in mathematics and the Ph.D. degree in control theory (both summa cum laude) from the Eindhoven University of Technology (TU/e), The Netherlands, in 1995 and 1999, respectively. From 2000 to 2004, he was with the Electrical Engineering Department, TU/e, as an assistant professor, and from 2004 to 2006 with the Embedded Systems Institute (ESI) as a research fellow. Since 2006, he has been with the Department of Mechanical Engineering, TU/e, where he is currently a Full Professor. He held visiting professor positions at the Swiss Federal Institute of Technology (ETH), Switzerland (2001) and at the University of California at Santa Barbara (2008). In 2004, he worked also at the company Océ, the Netherlands. His current research interests include hybrid and cyber–physical systems, networked and event-triggered control systems and constrained systems including model predictive control. Dr. Heemels served/s on the editorial boards of Automatica, Nonlinear Analysis: Hybrid Systems, Annual Reviews in Control, and IEEE Transactions on Automatic Control. He was a recipient of a personal VICI grant awarded by STW (Dutch Technology Foundation). He is a Fellow of the IEEE. He is currently chair of the IFAC Technical Committee on Networked Systems.

Henk Nijmeijer (1955) is a full professor at Eindhoven, and chairs the Dynamics and Control group. He has published a large number of journal and conference papers, and several books, and is or was at the editorial board of numerous journals. He is an editor of Communications in Nonlinear Science and Numerical Simulations. He is a fellow of the IEEE since 2000 and was awarded in 1990 the IEE Heaviside premium. He is appointed honorary knight of the golden feedback loop (NTNU) in 2011. He is since 2011 an IFAC Council Member. Per January 2015 he is scientific director of the Dutch Institute of Systems and Control (DISC). He is recipient of the 2015 IEEE Control Systems Technology Award and a member of the Mexican Academy of Sciences.

Nathan van de Wouw obtained his M.Sc.-degree (with honours) and Ph.D.-degree in Mechanical Engineering from the Eindhoven University of Technology The Netherlands, in 1994 and 1999, respectively. He currently holds a full professor position at the Mechanical Engineering Department of the Eindhoven University of Technology, the Netherlands. Nathan van de Wouw also holds an adjunct full professor position at the University of Minnesota, U.S.A. He has been working at Philips Applied Technologies, The Netherlands, in 2000 and at the Netherlands Organisation for Applied Scientific Research, The Netherlands, in 2001. He has been a visiting professor at the University of California Santa Barbara, U.S.A., in 2006/2007, at the University of Melbourne, Australia, in 2009/2010 and at the University of Minnesota, U.S.A., in 2012 and 2013. He has held a (part-time) full professor position at the Delft University of Technology, The Netherlands, from 2015 to 2019. He has published the books 'Uniform Output Regulation of Nonlinear Systems: A convergent Dynamics Approach' with A.V. Pavlov and H. Nijmeijer (Birkhauser, 2005) and 'Stability and Convergence of Mechanical Systems with Unilateral Constraints' with R.I. Leine (Springer-Verlag, 2008). In 2015, he received the IEEE Control Systems Technology Award "For the development and application of variable-gain control techniques for high-performance motion systems".